Connecting Molecular Conformation to Aggregation in P3HT Using Near Edge X-ray Absorption Fine Structure Spectroscopy

Stephen G, Urquhart,[a,*] Mercedes Martinson,[a] Shaylin Eger,[a] Victor Murcia,[b] Harald Ade,[d] Brian A. Collins[b,c]

a. Department of Chemistry, University of Saskatchewan, Treaty Six Territory, Saskatoon, SK, Canada
b. Materials Science and Engineering Program, Washington State University, Pullman, WA
c. Department of Physics and Astronomy, Washington State University, Pullman, WA
d. Department of Physics, North Carolina State University, Raleigh, NC

Abstract

Carbon 1s Near Edge X-ray Absorption Fine Structure (NEXAFS) and UV-vis spectroscopy are used to examine differences between highly aggregated and poorly aggregated forms of the polymer poly(3-hexylthiophene) (P3HT), based on as-cast and annealed regio-random and regio-regular P3HT samples. UV-vis spectra show characteristic signatures of unaggregated P3HT in regio-random P3HT, and of H-aggregation in regio-regular P3HT samples. Distinct spectroscopic differences, including energy shifts, are observed in the NEXAFS spectra of aggregated P3HT relative to the unaggregated forms. These differences are reproduced with Transition – Potential Density Functional Theory (TP-DFT) calculations which explore aggregation and molecular confirmation. Differences in the NEXAFS spectra of P3HT are assigned to thiophene backbone twisting in the unaggregated forms of P3HT, and to various degrees of chain planarization in aggregated forms of P3HT that also correlate to the exciton bandwidth. These results open up the prospect of charactering conformation and related difficult to assess structural details through NEXAFS spectroscopy and correlative theory and electronic structure analysis.

* Corresponding author: Stephen.urquhart@usask.ca

Introduction

Semiconducting conjugated polymers are primary candidates for use as active components in printable electronics. Since their optoelectronic properties are highly dependent on details of their semicrystalline ordering and/or molecular conformation, intense research continues into resolving their structure-property relationships. Many fundamental studies have focused on the archetypical polymer poly(3-hexylthiophene) (P3HT) where X-ray diffraction and optical absorption and emission spectroscopy studies have shown that chain aggregation, conjugation and crystalline packing are closely linked to charge carrier mobilities within polymer-based field effect transistors.[1-2] Further study of this material in organic solar cells has demonstrated similar correlations with charge generation and device efficiency.[3-4] In particular, intramolecular ("J-like") versus intermolecular ("H-like") electronic coupling are important in determining these properties and have been linked to molecular conformation and crystallinity.[2, 5] Measurement techniques capable of resolving the ordered state of conjugated polymers are important to the continuing progress in the field.

Near edge X-ray absorption fine structure (NEXAFS) spectroscopy can be used to study ordering in conjugated polymers. NEXAFS spectra of organic molecules are sensitive to intramolecular structure, orientation, and bonding but have relatively weak sensitivity to intermolecular order. For example, the distinctive Carbon 1s $\rightarrow \pi^*$ transition in unsaturated organic molecules is highly sensitive to functional group identity and substitution.[6-7] NEXAFS transitions can be used to determine molecular orientation within a sample and can be used to determine relative molecular orientations between different chemical bonds within a molecule.[8] This orientation sensitivity has been recently used to connect structure-property relationships in organic electronics, via spectroscopy and spectroscopically-resolved scattering experiments.[9-11] NEXAFS spectroscopy is also sensitive to conjugation and delocalization in extended unsaturated

systems, where the electronic structure is modified by the dihedral angles connecting these unsaturated thiophene moeties.[12-13]

Intermolecular interactions will have a weaker effect on NEXAFS spectra. Distinct Rydberg transitions observed in the gas phase NEXAFS spectra of simple molecules are broadened and shifted to higher energy in the condensed phase NEXAFS spectra of the same species.[14-15] This effect is attributed to Rydberg quenching in the condensed phase.[15-16] A small red-shift is observed in the Carbon 1s → π* transition for pyridine[17] and benzene clusters,[18] relative to their gas phase NEXAFS spectra. This effect is attributed to dynamic stabilization, in which the core excited cluster deforms to trap the core excited molecule in a modified geometry.[17] We hypothesize that NEXAFS spectroscopy could be sensitive to interchain π-π interactions and aggregation in polymers used for organic electronic materials, such as P3HT. NEXAFS spectroscopy will also be sensitive to the planarization of the P3HT backbone during aggregation, as π-conjugation between adjacent thiophene rings will evolve as thiophene rings become coplanar.

The structure of regio-regular (RR) and regio-random (RRa) P3HT in solution and as an unaggregated solid is characterized by non-planarity of adjacent thiophene rings,[19-20] with a typical dihedral angle of ~40°.[20] Steric interactions between adjacent hexyl groups in head-to-head linkages in RRa-P3HT will lead to non-planarity and will prevent aggregation of the polymer into ordered structures. The ordered structure of RR-P3HT (in H aggregate form) is characterized by planarity of the thiophene rings along the P3HT backbone, π-stacking between adjacent P3HT chains, and crystallization of the hexyl side groups.[21-22] Interchain interactions in P3HT arise from the co-facially aligned thiophene rings on adjacent polymer chains. The short spacing between thiophene rings on adjacent chains (as short as 3.4 Å, with tilted thiophene rings in epitaxially growth P3HT,[21] or 3.9 Å between planar thiophene rings in bulk P3HT samples)[22] permits charge and exciton transfer. H-aggregate Coulombic coupling has been shown to dominate optical

absorption and emission properties involving Frenkel excitons of importance to charge generation in organic photovoltaics.[23-24]

NEXAFS spectroscopy can probe the π* lowest unoccupied molecular orbital (LUMO) in a site-specific manner, as small chemical shifts can lead to distinct Carbon 1s → π* transitions for the different carbon atoms on the thiophene ring. These transitions, in turn, can be sensitive to intermolecular π/π interactions and electronic coupling of adjacent thophene groups as the chain planarity changes. Solid state P3HT films are composed of crystalline and noncrystalline phases; the latter involves entangled chains that tie neighboring crystals together. The interplay of ordered and disordered regions gives rise to macroscopic properties, motivating the development of tools sensitive to intermolecular interactions and chain planarity. NEXAFS could reveal insights into critical structure-property relationships in P3HT.

NEXAFS spectroscopy of P3HT has been examined previously by several groups.[9, 25-33] Many studies use NEXAFS to study the orientation of P3HT chains.[9, 25, 27, 32-33] MacLeod et al. examined the HOMO-LUMO gap in P3HT, [6,6]-phenyl-C_{61}-butyric acid methyl ester (PCBM), and P3HT/PCBM blends by NEXAFS, X-ray emission spectroscopy, and DFT calculations.[26] They attributed changes in the HOMO-LUMO gap to changes in ordering with annealing. Tillack et al., Germack et al. and Xue et al. used different NEXAFS detection methods to examine different aspects of the surface and bulk chemistry and vertical stratification in P3HT/PCBM blends;[28, 33-34] Collins, Ade and coworkers have studied the X-ray microscopy of P3HT/PCBM blends for similar goals.[29-31] Ho et al. examined NEXAFS spectroscopy of P3HT at air and buried interfaces as a function of solvent.[32] With the support of *ab inito* Z+1 calculations, their work showed a red-shift of the Carbon 1s → π* band that was correlated to stronger π/π interactions.

In this study, P3HT polymers with two different degrees of regio-regular character (92% and 98% RR-P3HT) and regio-random P3HT (RRa-P3HT), in as-cast and annealed forms, were

examined by UV-vis and NEXAFS spectroscopy. UV-vis spectra show characteristic differences due to aggregation in the regio-regular polymer, consistent with literature. The experimental NEXAFS spectra show a distinct change in the Carbon 1s → π* band which is correlated with the degree of aggregation quantified by the exciton bandwidth from Spano model fits. These NEXAFS spectra are interpreted in a site-specific manner with the aid of density functional theory (DFT) spectroscopic simulations of isolated and cluster P3HT models which indicate that the π* band is sensitive to chain planarity and therefore electronic conjugation. This is the first study we are aware of that interprets through DFT calculations the experimental NEXAFS spectroscopy for different P3HT grades and processing conditions and correlates these results with Spano analysis of UV-vis spectroscopy,[2-3, 35] to reveal sensitivity of NEXAFS to molecular conformation and aggregation.

2. Experimental

2.1 Polymer Materials and Preparation

Three different P3HT materials were used for NEXAFS and UV/vis spectroscopy in this work: regio-random P3HT (RRa-P3HT), and regio-regular P3HT (RR-P3HT) with 92% and 98% regio-regularity. RRa-P3HT and 98% RR-P3HT was purchased from Sigma Aldrich and the 92% RR-P3HT was purchased from Rieke Metals. Chlorobenezene was purchased from Sigma Aldrich. Glass substrates were cleaned via sonication in separate baths of detergent, deionized water, isopropanol, and acetone with a subsequent 15 minute UV-ozone treatment. Sodium polystyrenesulfonate (NaPSS) films were spincast from water and dried at 120C in a vacuum oven for 30 minutes. Such films were used as a water-soluble sacrificial layer beneath the P3HT film to release the P3HT film from the substrate for transmission NEXAFS measurements. P3HT films were prepared by spincasting the polymer from chlorobenzene solvent onto the NaPSS/glass substrates with a thickness of ~100 nm. Annealed samples were annealed at 160°C (NIST-calibrated surface

thermometer) for 10 min on a Petri dish-covered hotplate in an inert N_2 glovebox environment (1 ppm O_2 and H_2O).

2.2 UV/Vis spectroscopy

UV-vis spectroscopy was acquired on a Cary 50 instrument in transmission mode. Spectra were converted to optical density using Beer's Law formula $OD = log(I_0/I)$.

2.3 NEXAFS Spectroscopy

Carbon 1s NEXAFS spectroscopy was acquired in transmission on the Scanning Transmission X-ray Microscope (STXM) at BL 5.3.2.2 of the Advanced Light Source.[36] The same films used in UV/vis spectroscopy were released from their substrates by floating in deionized water and suspending them on copper grids. Measurements were completed in 1/3 atmosphere of He in the sample chamber and ~1 meter of the beamline flooded with 0.6 Torr of N_2 to reduce higher order X-ray spectral contamination. The $I_0(E)$ spectrum was recorded through an open area adjacent to the film and spectra were converted to optical densities through the Beers' Law formula, $OD = ln(I_0/I)$. Spectra were calibrated to the 3s and 3p Rydberg transitions of CO_2 gas leaked into the chamber, and set to literature values.[37] Background intensities and detector nonlinearity was corrected via previously demonstrated procedures.[31] For each sample, at least three spectra were acquired on different parts of the sample to assure they were reproducible and representative of the entire film. Each spectrum was measured by defocusing the beam until no damage could be detected upon a subsequent image at 285.3 eV.

3. Computational

The NEXAFS spectra of P3HT were simulated with DFT calculations. Calculations were performed for an isolated model of the RR-P3HT chain, a model of a RR-P3HT in a crystalline environment, and single chains with simulated non-planar RR and RRa-P3HT structures.

Several approximations were used to prepare appropriate structural models for an isolated P3HT chain and for P3HT in a crystalline environment. As P3HT is a semi-crystalline polymer, a definitive structure from single crystal X-ray diffraction is not available. Dudenko et al. used X-ray diffraction, solid-state NMR spectroscopy, and DFT calculations to define an abstracted single crystal RR-P3HT structure (e.g., a, b, c, α, β, γ, and fractional coordinates).[22] Along with RR-P3HT, this study provided a simplified structure where the hexyl group is replaced by a methyl group (RR-P3MT, for regio-regular poly(3-methylthiophene). Later in this work, we demonstrate that the low energy Carbon 1s → π* transitions associated with the thiophene ring are sensitive to intermolecular interactions and to changes in the P3HT chain planarity. As the π*-structure of the thiophene ring will not be strongly perturbed by the identity of the alkyl substituent (methyl vs. hexyl), the use of the methyl-functionalized model is a suitable approximation. The alkyl group contribution to the NEXAFS spectra appears at 287-288 eV, well above from the π* band of the thiophene ring.

Specific structures were generated from the RR-P3MT structures of Dudenko et al.[22] using a python script that uses the structure manipulation and visualization routines of the Atomic Simulation Environment (ASE).[38] Specific structures (isolated RR-P3MT chains and model clusters of RR-P3MT chains) can be extracted the extended RR-P3MT crystal structure. The end of these oligimer chains was terminated with a methyl group.

A second approximation replaces an infinite polymer chain by a finite-length oligomer model. As NEXAFS transitions are localized by the core hole, shorter oligomer models can be used, even for polymers with extensive π-conjugation.[12, 39-40] To determine the appropriate oligomer

length to simulate the P3HT polymer, TP-DFT simulations of the Carbon 1s NEXAFS spectra of the *central* thiophene ring in the methyl-terminated P3MT trimer, pentamer, septamer, and nonamer were examined (data shown in Supporting Information, Figure S1). These data show that the simulated spectrum of the P3MT pentamer, septamer, and nonamer are similar, and that the P3MT pentamer has an appropriate length to simulate the P3HT NEXAFS spectrum, particularly for the two lowest energy π* transitions. In subsequent simulations, calculations are only performed for the central thiophene ring of the P3MT oligomer.

The effect of P3HT chain planarity was examined by systematically varying the S-C-C-S dihedral angles in the RR-P3MT backbone, using the isolated RR-P3MT pentamer as a starting point. Structures were generated from the near-planar RR-P3MT chain structure (shown in the top of Scheme 1), and for the~180° degree S-C-C-S dihedral angle modified by +/- 20°, +/- 40° and +/- 60°; with angles set to alternate, or combine to form a left-or-right handed corkscrew structure.

In the aggregated RR-P3HT structure, inter-chain interactions are hypothesized to further perturb the NEXAFS spectra. To explore these effects, a model was generated to simulate the crystalline environment of the P3HT polymer. This model consists of a central RR-P3MT pentamer oligomer sandwiched between two RR-P3MT trimer oligomers. Shorter trimers are used for the outer groups, as the NEXAFS calculation is performed for the central thiophene of the central P3MT pentamer, and chain conjugation of the adjacent chains is not expected to be as significant. This trimer / pentamer / trimer structure was used to decrease the size of the model and the complexity of the subsequent DFT simulations. This structure was extracted from the abstracted RR-P3MT crystal structure of Dudenko et al.[22] and therefore is expected to have the appropriate interchain spacing (3.9 Å) and thiophene herringbone structure found in the P3HT solid. Schematics for a single methyl terminated RR-P3MT pentamer oligomer and methyl terminated trimer/pentamer/trimer solid structure are presented in **Scheme 1**.

Regio-regular P3HT (RR-P3HT) chains will consist exclusively of head-to-tail combinations of the 3-hexyl thiophene monomers, while regio-random P3HT (RRa-P3HT) will have random head-to-head and head-to-tail combinations of the 3-hexyl thiophene monomers. As this structural variation may lead to differences in the NEXAFS spectra, the contribution of head-to-head bonding was explicitly modeled. The isolated P3MT chain structure (top of Scheme 1) was modified to create a head-to-head (H2H) combination between the second and third thiophene ring, by moving the methyl group in the second thiophene ring to the site identified by an asterisk in Scheme 1. Calculations were performed for the central thiophene ring in this structure.

Carbon 1s NEXAFS simulations were obtained from DFT calculations using the PBE correlational functional.[41] Spectroscopic simulations were obtained using the half-core-hole (HCH) transition-potential density functional theory (TP-DFT) method,[42] using the deMon2K code (version 4.2.1).[43] Equivalent core potentials for all heavy atoms (C and S) except for the core excited atom. The IGLO-III basis set[44] is used on the core excited carbon atom, augmented by the XAS-I basis set.[45-46] Simulated spectra were generated from these calculations by using a 0.2 eV wide Gaussian line shape for each calculated core excitation transition, using the XAS code accompanying deMon2k.

4. Results and Discussion

UV-vis spectra of RRa-P3HT, 92% RR-P3HT and 98% RR-P3HT, in as cast and annealed forms, are presented in **Figure 1 (top)**. The RRa-P3HT spectra show a broad featureless maximum at higher energy (~2.75 eV) while the RR-P3HT spectra show a structured maximum around 2.05 eV. Clark et al.[47] observed the higher energy feature in conditions where aggregation is not present, in highly dilute P3HT solutions (0.0001 wt %) and in less-dilute (1%) P3HT solutions at an elevated temperature (70°C). As temperatures in those experiments approached ambient, the UV-vis spectra of the 1% P3HT solutions shifted to lower energy and show structure, indicating that P3HT

crystallites formed in solution.[47] Reflecting on our data in Figure 1, the RRa-P3HT species (annealed and as-cast) do not show evidence of aggregation, while the RR-P3HT samples (92% and 98% regio-regularity), annealed and as-cast, show the distinct H-aggregation signature in their UV-vis spectra.[47]

In the UV-vis spectra of the RR-P3HT spectra, the 0-0 absorbance (narrow band at ~2.05 eV) increases in intensity from as-cast to annealed in 92% RR, and then further for as-cast and annealed 98% RR-P3HT. The UV-vis spectra of the four RR-P3HT polymers were fit to the Spano model to determine exciton bandwidth and degree of aggregation.[2-3, 35] These results are presented in **Table 1**, and plots of the fits are presented in Supporting Information, **Figure S2**. The degree of aggregation is similar for all of the RR P3HT species (41.4 – 42.9%). The exciton bandwidth decreases linearly as the degree of regio-regularity increases (160 → 117 meV, for 92 → 98% regio-regularity) and with annealing (117 → 96 meV for 98% RR-P3HT). These changes are consistent with the expected increase in conjugation length as the thiophene rings in the polymer backbone become more planar, with annealing and with increased regio-regularity. It is interesting that the exciton bandwidth is strongly affected by increasing regio-regularity from 92% to 98% while the % aggregates remains constant, as one would think that an increased volume fraction of crystallized polymer would result in a smaller volume fraction of amorphous/non-aggregated material.

Experimental Carbon 1s NEXAFS spectra of RRa-P3HT, 92% RR-P3HT and 98% RR-P3HT, in as cast and annealed condition, are presented in **Figure 1 (bottom)**. The presentation in Figure 1 examines the lower energy Carbon 1s → π* transition of the thiophene ring; full spectra are included in Supporting Information, **Figure S3**. Plots of the fits of the π* band to Gaussian lineshapes are presented in **Figure S4**; results of fits are presented in **Table S1** (Supporting Information). The NEXAFS spectra of P3HT presented in this paper are consistent with those in the majority of the literature,[9, 25, 27-34] with an asymmetric carbon 1s → π* peak, an alkyl carbon 1s →

$\sigma^*_{C\text{-}H}$ peak intensity commensurate with the P3HT composition, and with expected differences due to experimental energy resolution or linear dichroism.

The π* band for thiophene contains 2-3 features: the most intense feature (C) at ~285.2 eV, and 1-2 shoulders, labelled as (A) and (B), at lower energy (284.4 – 284.8 eV). The broad low energy feature in RRa-P3HT is labelled (A'). Carbon 1s → $\sigma^*_{C\text{-}H}$/3p Rydberg transitions of the hexyl substituent dominate the spectra above 287 eV, so this energy range is not discussed further.

In the NEXAFS spectra of RRa-P3HT, the broad π* band (C) shifts to higher energy with annealing, and a broad band (A') fills in below (C). The NEXAFS spectrum of as-cast 92% RR-P3HT is similar to as-cast RRa-P3HT, although feature (C) is slightly broader in the RRa-P3HT sample. The shift of feature (C) to higher energy also occurs in 92% RR-P3HT (~20 meV) with annealing. Unlike annealed RRa-P3HT, a clearly resolved band (B) appears between (A) and (C) in the NEXAFS spectrum of annealed 92% RR-P3HT. In 98% RR-P3HT, bands (A), (B) and (C) are observed in the as cast sample, and there is relatively little change with annealing.

The π* band features identified in Figure 1 are interpreted with the aid of DFT calculations. **Figure 2** presents a TP-DFT NEXAFS simulation of the Carbon 1s → π* band in the NEXAFS spectrum of the isolated RR-P3HT model (central ring of the P3MT pentamer; head-to-tail structure; H2T) as well as P3HT models that simulate head-to-head (H2H) structures, with different chain conformations. These simulations are compared to the experimental carbon 1s NEXAFS spectrum of annealed 98% RR-P3HT, and as-cast and annealed RRa-P3HT.

We will first focus on the RR-P3HT simulation (e.g. H2T, for 'head to tail' bonding in regio-regular P3HT). There is excellent agreement between the P3HT simulation and the 98% RR-P3HT experimental spectrum. The simulation shows that the lowest energy transition (A) is assigned as a Carbon → π* transition originating at the 4-position of the thiophene ring; the second Carbon → π* transition (B) is assigned as a Carbon → π* transition originating at the 3-position; and the broad

band (C) is assigned as an overlap of Carbon → π* transitions from thiophene C-R ring sites (2-position and 5-position).

We will now examine the variation in P3HT spectra as a function of regio-regular and regio-random character. Significant differences are observed between the experimental NEXAFS spectra of RR-P3HT and RRa-P3HT. The well-defined low energy features (A) and (B) are obscured (A') in RRa-P3HT, and feature (C) is significantly broadened as regio-regularity was lost. To understand these differences, we examine the effect of regio-random bonding on the P3HT NEXAFS spectra. Regio-random bonding will have a random distribution of head-to-head (H2H) and head-to-tail (H2T) backbone bonding. Steric interference between hexyl side groups in head-to-head combinations will also make it more difficult for the thiophene rings to adopt a planar geometry. **Figure 2** includes simulations of the Carbon 1s NEXAFS spectrum of four head-to-head (H2H) models (planar, and with 20°, 40° and 60° additions to the ~180° S-C-C-S dihedral angles in planar P3HT). These simulations are compared to that of the planar H2T P3HT model. When examining the head-to-tail and head-to-head planar structures, we see that the lowest energy carbon 1s → π* transitions (3- and 4-positions) shift to higher energy for the head-to-head models. Band (C) broadens in the head-to-head model, as the carbon 1s → π* transition from the 5- and 2-positions are separated in energy. Steric hindrance of hexyl groups on adjacent 'head' groups will force RRa-P3HT into non-planar geometries; Figure 2 shows that the π* transition in non-planar head-to-head models will be shifted to higher energy as the chains become less planar. As RRa-P3HT will contain a random mixture of head-to-head and head-to-tail thiophene backbone bonding, its spectrum will be an average of these two models. The broadness of feature (C) in the RRa-P3HT model therefore arises from the separation of contributions from positions 2- and 5-, a blue shift of the contribution from the 3-position, and the likely range of dihedral angles along the P3HT backbone.

With annealing, feature (C) in the NEXAFS spectra of RRa-P3HT shifts to higher energy and narrows. This is attributed a decrease in the range of thiophene dihedral angles, while they remain non-planar. In the NEXAFS simulations of head-to-head (H2H) P3HT models, the lowest energy carbon 1s → π* transition (4) shifts to higher energy as the non-planarity increases, with a significant jump in energy between 40° and 60° dihedral angles. The carbon 1s → π* transitions associated with band (C) coalesce as the dihedral angles increase, as conjugation between adjacent thiophene rings is 'cut off'. Below (Figure 3), we will see that the non-planar H2T model behaves similarly. As the energy scales of simulation and experiment are relatively well matched, the 40° tilt angle model is the best match for band (C): band (C) in the 20° tilt H2H model and the 60° tilt H2H model appear at either too low or too high energy. Based on these results, we conclude that annealing causes the wide range of tilt angles to converge to a narrower range around 40°. This result provides additional experimental confirmation of the model of Khlaifia et al.[20]

The relative broadness of band (C) in as cast 92% RR-P3HT is similar to that of as cast RRa-P3HT. However, this broadness cannot be attributed to the contribution of head-to-head bonding combinations, as there are relatively few head-to-head combinations in this polymer (92% RR means 8% RRa, or ~4% head-to-head combinations). The narrowing of band (C) with annealing indicates a decrease in the range of dihedral angles with annealing. **Figure 3** compares the DFT simulations of the carbon 1s NEXAFS spectra of the central thiophene ring in the RR-P3HT model (P3MT pentamer) as a function of non-planarity of the thiophene rings; **Figure S5** in the Supporting Information presents the energy of the four lowest carbon 1s → π* transitions as a function of deviation from planarity. Blue shifts in the low energy carbon 1s → π* transitions (from the 3- and 4-position ring sites) are observed with increased non-planar angle; at a 40° modification to the dihedral angle, band (B) starts to overlap with band (C). On the basis of these results, the broadness of unannealed 92% RR-P3HT is attributed to a range of thiophene-thiophene dihedral angles in the unannealed polymer. With annealing, these rings become planar. The propensity for the RR-P3HT

polymer to become planar and the RRa-P3HT to be affected by steric hindrance and remain non-planar with annealing is explored through a Walsh diagram. **Figure S6** in the Supporting Information shows that the H2T (RR-P3HT) model has a deeper energy minimum centered at planarity than the H2H (RRa-P3HT) model.

The exciton bandwidth (from Spano fits of the UV-vis spectra) can be related to the P3HT chain conjugation length; longer conjugation length leads to a smaller exciton bandwidth. Only peak (A) is well defined in as cast 92% RR-P3HT; this sample also has the largest exciton bandwidth or the shortest conjugation length. As the 92% RR-P3HT sample is annealed, peak (B) becomes defined above peak (A), and the exciton bandwidth decreases. The conjugation length is associated with the relative planarity of thiophene rings along the P3HT chain. Based on these results, planarity is the lowest in the as-cast 92% RR-P3HT sample, and the backbone planarity and conjugation improves with annealing. Our DFT calculations predict that the energy of the lowest carbon 1s → π* transitions (sites 4 and 2) will decrease as the chain becomes more planar. This is observed in Figure 4(b), in direct correlation to the decreasing exciton bandwidth, which is indicative of chain planarity. In the NEXAFS spectra of 98% RR-P3HT sample, peaks (A) and (B) are clearly observed, and do not appear to change with annealing or show a further decrease in exciton bandwidth.

At this point, we assign the NEXAFS spectrum of un-aggregated P3HT (as-cast and annealed RRa-P3HT and as-cast 92% RR-P3HT) as a broad lower energy feature (A') arising from a carbon 1s → π* transition arising from the C-H ring site (4-position), where the broadness is attributed to energy shifts due to the range of thiophene/thiophene dihedral angles. The broadness of feature (C) is attributed to the overlap of carbon 1s → π* transitions arising from ring sites 2-, 3- and 5-position, broadened by the range of dihedral angles and the fraction of head-to-head linkages in RRa-P3HT. With annealing, 92% RR-P3HT adopts the characteristic spectrum of H-aggregated

P3HT, while RRa-P3HT is unable to aggregate due to steric interference of hexyl groups, from the random fraction of head-to-head linkages. Nevertheless, the range of dihedral angles appears to narrow.

Figure 4(a) presents disorder parameters (based on the Spano and NEXAFS peak widths) versus sample, in order of increasing polymer order. The degree of disorder observed by UV-vis and NEXAFS spectroscopy both decrease monotonically as the sample order increases. A factor of 2 collapses both sets of data onto one trend with NEXAFS peak widths consistently twice that of Spano peak widths. **Figure 4(b)** presents a comparison of NEXAFS peak energies for the two lowest energy π* transitions (A and B) with the UV-vis-derived exciton bandwidths. Both the π* transition energies and the exciton bandwidth decrease as the order increases. This is consistent with the results from our DFT calculations that shows decreasing transition energies that result from planarization of the P3HT chain, which should give rise to longer conjugation lengths and therefore smaller exciton bandwidths. Remarkably, the amount of decrease for both measures (~20 meV/sample) is also the same, and again all traces collapse onto one trend, this time with no scale factor but only a rigid shift in energy. Deviations in this correlation occur with the 98% RR-P3HT where NEXAFS peak positions stabilize rather than continue to decrease with the exciton bandwidth. The decrease in exciton bandwidth indicates an increase in conjugation length (i.e. electron delocalization) along the chain. A stabilization of the NEXAFS peaks with increasing UV-vis conjugation length could be due to the increased localization of the π* orbital in the presence of the core hole in NEXAFS measurements.[12, 48] NEXAFS appears to become insensitive to further ordering below an exciton bandwidth of ~130 meV.

The question of the effect of π/ π interactions with aggregation arises in response to predictions and observations in the literature.[17-18, 32, 49] **Figure 5** explores the variation of the Carbon 1s NEXAFS simulations of an isolated P3MT pentameter chain, and an aggregated P3MT

model based on the solid structure of Dudenko et al.[22] (see Scheme 1; 3.9 Å ring separation). A clear red shift is observed of all carbon 1s → π* transitions upon aggregation, consistent with the calculations of Ho et al.[32] This indicates that the energy and form of the π* transitions in P3HT are defined not only by ring planarity, but also by the ring-ring interactions between adjacent chains. In their recent study of paracyclophanes in which the phenyl/phenyl ring separation was rigorously controlled , Perera and Urquhart demonstrated that this 'red shift' was due to π/ π interactions between adjacent aromatic groups.[49] These π/ π interactions become more significant at distances smaller than the van der Waals separation for carbon (two times the van der Waals radius, or 3.4 Å), but this effect persists weakly at larger ring separations.[49] Spectroscopic fits presented in Table 2 show a red shift of a ~10 meV between peak (A') in RRa-P3HT and (A) in RR-P3HT, and a narrowing of peak (A) with annealing. This is consistent with a red-shift due to π/π interactions, which will be comparatively weak due to the 3.9 Å chain separation in the Dudenko model.[22] A larger shift should be observed in epitaxially growth P3HT, which has a 3.4 Å ring separation.[22]

Conclusions

We have correlated features observed in the NEXAFS and UV/vis spectra of P3HT with varying degrees of order as a consequence of regio-regularity and thermal treatment. TP-DFT calculations enable definitive assignment of NEXAFS features to carbon 1s → π* transitions to specific carbon atoms in the thiophene ring. These calculations aid in the interpretation of the NEXAFS spectra to explore chain conjugation, planarity, and regio-regularity individual P3HT chains, and π/ π interactions in solid P3HT. Our results confirm the non-planar structural model for RRa-P3HT and provide evidence for a narrowing of tilt angles around 40° in annealed RRa-P3HT. In RR-P3HT increased regio-regularity leads to increased conjugation as the thiophene backbone becomes planar. A correlation between the narrowed exciton bandwidth and the lowest carbon 1s → π* transition energies is observed, indicating these energies are indeed sensitive to both planarity and

electronic conjugation. A weak modification to the π* band occurs due to π/π interactions occurs in the most ordered thiophene samples.

These results and analysis show that NEXAFS spectroscopy is sensitive to conformation and aggregation in unsaturated polymers such as P3HT, particularly when performed in correlation with high-quality calculations and complementary structural and spectroscopic analysis. This approach could be useful for other organic electronic materials, where conformation and packing are important drivers of device properties.

Supporting Information

The supporting information is available free of charge on the ACS Publications website at DOI: xxx.

- Chain length dependence in the simulated NEXAFS of P3MT models; results of fits of UV-vis spectra to the Spano model; long energy range experimental NEXAFS spectra of P3HT species; results of fits of the NEXAFS π* band (fit results and plots); energy trend for lowest π* band for P3HT model planarity; total energy as a function of P3HT model planarity.

Acknowledgements

SGU is supported by the Nature Sciences and Engineering Research Council (Canada). HA is supported by the US Department of Energy, Office of Science, Basic Energy Science, Division of Materials Science and Engineering under Contract DE-FG02-98ER45737. NEXAFS measurements were performed at the Advanced Light Source, which is supported by the Director, Office of Science, Office of Basic Energy Sciences, of the U.S. Department of Energy under Contract No. DE-AC02-05CH11231. This research was enabled in part by support provided by WestGrid (www.westgrid.ca) and Compute Canada Calcul Canada (www.computecanada.ca), and University

of Saskatchewan HPC resources.

Figure Captions

Figure 1: (top) UV-vis spectra of regio-random poly(3-hexyl thiophene (RRa-P3HT; green traces) , 98% regio-regular poly(3-hexyl thiophene) (RR-P3HT; blue traces) in as cast and annealed form, and 92% RR-P3HT, in annealed form (red trace). (bttom) Carbon 1s → π* band of the NEXAFS spectra of regio-random poly(3-hexyl thiophene (RRa-P3HT; green traces) , 98% (blue traces) and 92% (red traces) regio-regular poly(3-hexyl thiophene) (RR-P3HT), in as cast and annealed form. Transitions labelled (1), (1'), (2) and (3) are discussed in the text.

Figure 2: Transition-potential density functional theory (TP-DFT) simulation of the Carbon 1s → π* band of the NEXAFS spectra of planar RR-P3HT (head-to-tail; H2T) and planar and non-planar head-to-head (H2H) contributions for RRa-P3HT. These simulations were obtained from calculations for the central thiophene ring of the methyl terminated 3-methyl-thiophene pentamer. The numbering reflects the IUPAC atomic labels used in Scheme 1. These simulated spectra are compared to the experimental Carbon 1s NEXAFS spectra of annealed 98% regio-regular P3HT and as cast and annealed RRa-P3HT. The energy scales of the simulated spectra have been offset to align with the experimental data.

Figure 3: Comparison of transition-potential density functional theory (TP-DFT) simulation of the Carbon 1s → π* band of RR-P3HT models, in a planar geometry, and with alternating or consistent thiophene-thiophenedihedral angles. These simulations were obtained from calculations for the central thiophene ring of the methyl terminated 3-methyl-thiophene pentamer.

Figure 4: (a) Disorder parameters versus sample (AC = as cast; AN = annealed). UV-vis disorder values are from the Spano model (Gaussian $\sigma \times 2$; see table 1); NEXAFS disorder values are from the Gaussian σ of peaks A and B, from the fits (see Table S1). (b) Correlation of the exciton bandwidth (σ, see table 1) to the NEXAFS peak A and B energies (E_A and E_B; see Table S1). E_A and E_B are reduced by 284.35 eV and 284.66 eV, respectively. The first component in the two-component fit of peak C in RRa-P3HT is used as peak B in this figure.

Figure 5: Comparison of transition-potential density functional theory (TP-DFT) simulation of the Carbon 1s → π* band of the isolated and solid P3HT models to the experimental Carbon 1s NEXAFS spectra of annealed 98% regio-regular P3HT (RR-P3HT). The energy scales of the calculation have been offset to align with the experimental data.

Scheme 1: Molecular Diagram of the methyl terminated 3-methyl-thiophene pentamer (top) and the methyl terminated 3-methyl-thiophene pentamer sandwiched between two methyl terminated 3-methyl-thiophene trimer molecules (bottom). The IUPAC numbering for the central thiophene ring is shown for the methyl terminated 3-methyl-thiophene pentamer. The asterisk in the methyl terminated 3-methyl-thiophene pentamer indicates where the methyl group is moved for the head-to-head model for the simulation of the regio-random structure.

Table 1: Calculated Exciton Bandwidth, Gaussian Width and Degree of Aggregation

	Exciton bandwidth (meV)	σ (meV)	Aggregation (%)
92% RR-P3HT as cast	160(1)	80	42.3
92% RR-P3HT annealed	137(4)	75	42.9
98% RR-P3HT as cast	117(2)	71	41.5
98% RR-P3HT annealed	96(1)	71	41.4

a. Huang-Rhys parameter set to 1, assuming pure H-aggregates.

References:

1. Sirringhaus, H.; Tessler, N.; Friend, R. H. Integrated Optoelectronic Devices Based on Conjugated Polymers. *Science* **1998**, *280*, 1741-1744.
2. Clark, J.; Chang, J.-F.; Spano, F. C.; Friend, R. H.; Silva, C. Determining Exciton Bandwidth and Film Microstructure in Polythiophene Films Using Linear Absorption Spectroscopy. *Appl. Phys. Lett.* **2009**, *94*, 163306.
3. Turner, S. T.; Pingel, P.; Steyrleuthner, R.; Crossland, E. J. W.; Ludwigs, S.; Neher, D. Quantitative Analysis of Bulk Heterojunction Films Using Linear Absorption Spectroscopy and Solar Cell Performance. *Adv. Funct. Mater.* **2011**, *21*, 4640-4652.
4. Treat, N. D.; Shuttle, C. G.; Toney, M. F.; Hawker, C. J.; Chabinyc, M. L. In Situ Measurement of Power Conversion Efficiency and Molecular Ordering During Thermal Annealing in P3HT:PCBM Bulk Heterojunction Solar Cells. *J. Mater. Chem.* **2011**, *21*, 15224-15231.
5. Paquin, F.; Yamagata, H.; Hestand, N. J.; Sakowicz, M.; Bérubé, N.; Côté, M.; Reynolds, L. X.; Haque, S. A.; Stingelin, N.; Spano, F. C., et al. Two-Dimensional Spatial Coherence of Excitons in Semicrystalline Polymeric Semiconductors: Effect of Molecular Weight. *Phys. Rev. B* **2013**, *88*, 155202.
6. Cooney, R. R.; Urquhart, S. G. Chemical Trends in the near-Edge X-Ray Absorption Fine Structure of Monosubstituted and Para-Bisubstituted Benzenes. *J. Phys. Chem. B.* **2004**, *108*, 18185-18191.
7. Urquhart, S. G.; Ade, H. Trends in the Carbonyl Core (C 1s, O 1s) → π*C=O Transition in the near-Edge X-Ray Absorption Fine Structure Spectra of Organic Molecules. *J. Phys. Chem. B.* **2002**, *106*, 8531-8538.
8. Stöhr, J. *NEXAFS Spectroscopy*; Springer-Verlag Berlin Heidelberg, 1992; Vol. 25.
9. Germack, D. S.; Chan, C. K.; Hamadani, B. H.; Richter, L. J.; Fischer, D. A.; Gundlach, D. J.; DeLongchamp, D. M. Substrate-Dependent Interface Composition and Charge Transport in Films for Organic Photovoltaics. *Appl. Phys. Lett.* **2009**, *94*, 233303.
10. Collins, B. A.; Cochran, J. E.; Yan, H.; Gann, E.; Hub, C.; Fink, R.; Wang, C.; Schuettfort, T.; McNeill, C. R.; Chabinyc, M. L., et al. Polarized X-Ray Scattering Reveals Non-Crystalline Orientational Ordering in Organic Films. *Nat. Mater.* **2012**, *11*, 536-543.
11. Tumbleston, J. R.; Collins, B. A.; Yang, L.; Stuart, A. C.; Gann, E.; Ma, W.; You, W.; Ade, H. The Influence of Molecular Orientation on Organic Bulk Heterojunction Solar Cells. *Nat. Photonics* **2014**, *8*, 385-391.
12. Urquhart, S. G.; Hitchcock, A. P.; Smith, A. P.; Ade, H.; Rightor, E. G. Inner-Shell Excitation Spectroscopy of Polymer and Monomer Isomers of Dimethyl Phthalate. *J. Phys. Chem. B.* **1997**, *101*, 2267-2276.
13. Wang, J.; Cooper, G.; Tulumello, D.; Hitchcock, A. P. Inner Shell Excitation Spectroscopy of Biphenyl and Substituted Biphenyls: Probing Ring−Ring Delocalization. *J. Phys. Chem. A* **2005**, *109*, 10886-10896.
14. Urquhart, S. G.; Gillies, R. Rydberg−Valence Mixing in the Carbon 1s near-Edge X-Ray Absorption Fine Structure Spectra of Gaseous Alkanes. *J. Phys. Chem. A* **2005**, *109*, 2151-2159.
15. Urquhart, S. G.; Gillies, R. Matrix Effects in the Carbon 1s near Edge X-Ray Absorption Fine Structure Spectra of Condensed Alkanes. *J. Chem. Phys.* **2006**, *124*, -.
16. Schöll, A.; Fink, R.; Umbach, E.; Mitchell, G. E.; Urquhart, S. G.; Ade, H. Towards a Detailed Understanding of the NEXAFS Spectra of Bulk Polyethylene Copolymers and Related Alkanes. *Chem. Phys. Lett.* **2003**, *370*, 834-841.
17. Bradeanu, I. L.; Kosugi, N.; Flesch, R.; Rühl, E. Site-Dependent Spectral Shifts in Core-to-π* Excitations of Pyridine Clusters. *J. Phys. Chem. A* **2008**, *112*, 9192-9199.

18. Bradeanu, I. L.; Flesch, R.; Kosugi, N.; Pavlychev, A. A.; Ruhl, E. C 1s → π* Excitation in Variable Size Benzene Clusters. *Phys. Chem. Chem. Phys.* **2006**, *8*, 1906-1913.
19. Böckmann, M.; Schemme, T.; de Jong, D. H.; Denz, C.; Heuer, A.; Doltsinis, N. L. Structure of P3ht Crystals, Thin Films, and Solutions by Uv/Vis Spectral Analysis. *Phys. Chem. Chem. Phys.* **2015**, *17*, 28616-28625.
20. Khlaifia, D.; Ewels, C. P.; Massuyeau, F.; Chemek, M.; Faulques, E.; Duvail, J.-L.; Alimi, K. Unraveling the Real Structures of Solution-Based and Surface-Bound Poly(3-Hexylthiophene) (P3HT) Oligomers: A Combined Theoretical and Experimental Study. *RSC Adv.* **2016**, *6*, 56174-56182.
21. Kayunkid, N.; Uttiya, S.; Brinkmann, M. Structural Model of Regioregular Poly (3-Hexylthiophene) Obtained by Electron Diffraction Analysis. *Macromolecules* **2010**, *43*, 4961-4967.
22. Dudenko, D.; Kiersnowski, A.; Shu, J.; Pisula, W.; Sebastiani, D.; Spiess, H. W.; Hansen, M. R. A Strategy for Revealing the Packing in Semicrystalline Π-Conjugated Polymers: Crystal Structure of Bulk Poly-3-Hexyl-Thiophene (P3HT) *Angew. Chem., Int. Ed.* **2012**, *51*, 11068–11072.
23. Proctor, C. M.; Kuik, M.; Nguyen, T.-Q. Charge Carrier Recombination in Organic Solar Cells. *Prog. Polym. Sci.* **2013**, *38*, 1941-1960.
24. Tvingstedt, K.; Vandewal, K.; Zhang, F.; Inganäs, O. On the Dissociation Efficiency of Charge Transfer Excitons and Frenkel Excitons in Organic Solar Cells: A Luminescence Quenching Study. *J. Phys. Chem. C* **2010**, *114*, 21824-21832.
25. Salleo, A.; Kline, R. J.; DeLongchamp, D. M.; Chabinyc, M. L. Microstructural Characterization and Charge Transport in Thin Films of Conjugated Polymers. *Adv. Mater.* **2010**, *22*, 3812-3838.
26. McLeod, J. A.; Pitman, A. L.; Kurmaev, E. Z.; Finkelstein, L. D.; Zhidkov, I. S.; Savva, A.; Moewes, A. Linking the Homo-Lumo Gap to Torsional Disorder in P3HT/PCBM Blends. *J. Chem. Phys.* **2015**, *143*, 224704.
27. DeLongchamp, D. M.; Vogel, B. M.; Jung, Y.; Gurau, M. C.; Richter, C. A.; Kirillov, O. A.; Obrzut, J.; Fischer, D. A.; Sambasivan, S.; Richter, L. J., et al. Variations in Semiconducting Polymer Microstructure and Hole Mobility with Spin-Coating Speed. *Chem. Mater.* **2005**, *17*, 5610-5612.
28. Tillack, A. F.; Noone, K. M.; MacLeod, B. A.; Nordlund, D.; Nagle, K. P.; Bradley, J. A.; Hau, S. K.; Yip, H.-L.; Jen, A. K. Y.; Seidler, G. T., et al. Surface Characterization of Polythiophene:Fullerene Blends on Different Electrodes Using near Edge X-Ray Absorption Fine Structure. *ACS Appl. Mater. Interfaces* **2011**, *3*, 726-732.
29. Collins, B. A.; Gann, E.; Guignard, L.; He, X.; McNeill, C. R.; Ade, H. Molecular Miscibility of Polymer−Fullerene Blends. *J. Phys. Chem. Lett.* **2010**, *1*, 3160-3166.
30. Collins, B. A.; Tumbleston, J. R.; Ade, H. Miscibility, Crystallinity, and Phase Development in P3HT/PCBM Solar Cells: Toward an Enlightened Understanding of Device Morphology and Stability. *J. Phys. Chem. Lett.* **2011**, *2*, 3135-3145.
31. Collins, B. A.; Ade, H. Quantitative Compositional Analysis of Organic Thin Films Using Transmission NEXAFS Spectroscopy in an X-Ray Microscope. *J. Electron Spectrosc. Relat. Phenom.* **2012**, *185*, 119-128.
32. Ho, P. K. H.; Chua, L. L.; Dipankar, M.; Gao, X. Y.; Qi, D. C.; Wee, A. T. S.; Chang, J. F.; Friend, R. H. Solvent Effects on Chain Orientation and Interchain π-Interaction in Conjugated Polymer Thin Films: Direct Measurements of the Air and Substrate Interfaces by near-Edge X-Ray Absorption Spectroscopy. *Adv. Mater.* **2007**, *19*, 215-221.
33. Xue, B.; Vaughan, B.; Poh, C.-H.; Burke, K. B.; Thomsen, L.; Stapleton, A.; Zhou, X.; Bryant, G. W.; Belcher, W.; Dastoor, P. C. Vertical Stratification and Interfacial Structure in P3HT:PCBM Organic Solar Cells. *J. Phys. Chem. C* **2010**, *114*, 15797-15805.
34. Germack, D. S.; Chan, C. K.; Kline, R. J.; Fischer, D. A.; Gundlach, D. J.; Toney, M. F.; Richter, L. J.; DeLongchamp, D. M. Interfacial Segregation in Polymer/Fullerene Blend Films for Photovoltaic Devices. *Macromolecules* **2010**, *43*, 3828-3836.

35. Spano, F. C. Modeling Disorder in Polymer Aggregates: The Optical Spectroscopy of Regioregular Poly(3-Hexylthiophene) Thin Films. *J. Chem. Phys.* **2005**, *122*, 234701.
36. Kilcoyne, D.; Ade, H.; Attwood, D.; Hitchcock, A.; McKean, P.; Mitchell, G.; Monteiro, P.; Tyliszczak, T.; Warwick, T. A New Scanning Transmission X-Ray Microscope at the Als for Operation up to 2500 eV. *AIP Conf. Proc.* **2010**, *1234*, 465-468.
37. Ma, Y.; Chen, C. T.; Meigs, G.; Randall, K.; Sette, F. High-Resolution K-Shell Photoabsorption Measurements of Simple Molecules. *Phys. Rev. A* **1991**, *44*, 1848-1858.
38. Bahn, S. R.; Jacobsen, K. W. An Object-Oriented Scripting Interface to a Legacy Electronic Structure Code. *Comput. Sci. Eng.* **2002**, *4*, 56-66.
39. Urquhart, S. G.; Smith, A. P.; Ade, H. W.; Hitchcock, A. P.; Rightor, E. G.; Lidy, W. Near-Edge X-Ray Absorption Fine Structure Spectroscopy of MDI and TDI Polyurethane Polymers. *J. Phys. Chem. B.* **1999**, *103*, 4603-4610.
40. Giebler, R.; Schulz, B.; Reiche, J.; Brehmer, L.; Wühn, M.; Wöll, C.; Smith, A. P.; Urquhart, S. G.; Ade, H. W.; Unger, W. E. S. Near-Edge X-Ray Absorption Fine Structure Spectroscopy on Ordered Films of an Amphiphilic Derivate of 2,5-Diphenyl-1,3,4-Oxadiazole. *Langmuir* **1999**, *15*, 1291-1298.
41. Perdew, J. P.; Burke, K.; Ernzerhof, M. Generalized Gradient Approximation Made Simple. *Phys. Rev. Lett.* **1996**, *77*, 3865-3868.
42. Triguero, L.; Pettersson, L. G. M.; Ågren, H. Calculations of near-Edge X-Ray-Absorption Spectra of Gas-Phase and Chemisorbed Molecules by Means of Density-Functional and Transition-Potential Theory. *Phys. Rev. B* **1998**, *58*, 8097-8110.
43. Koster, A. M.; Geudtner, G.; Calaminici, P.; Casida, M. E.; Dominguez, V. D.; Flores-Moreno, R.; Gamboa, G. U.; Goursot, A.; Heine, T.; Ipatov, A., et al. *Demon2k*, Cinvestav, Mexico City 2011.
44. Huzinaga, S. Gaussian-Type Functions for Polyatomic Systems. 1. *J. Chem. Phys.* **1965**, *42*, 1293.
45. Ågren, H.; Carravetta, V.; Vahtras, O.; Pettersson, L. G. M. Direct, Atomic Orbital, Static Exchange Calculations of Photoabsorption Spectra of Large Molecules and Clusters. *Chem. Phys. Lett.* **1994**, *222*, 75-81.
46. Ågren, H.; Carravetta, V.; Vahtras, O.; Pettersson, M. L. G. Direct SCF Direct Static-Exchange Calculations of Electronic Spectra. *Theor. Chem. Acc.* **1997**, *97*, 14-40.
47. Clark, J.; Silva, C.; Friend, R. H.; Spano, F. C. Role of Intermolecular Coupling in the Photophysics of Disordered Organic Semiconductors: Aggregate Emission in Regioregular Polythiophene. *Phys. Rev. Lett.* **2007**, *98*, 206406.
48. Ågren, H.; Vahtras, O.; Carravetta, V. Near-Edge Core Photoabsorption in Polyacenes: Model Molecules for Graphite. *Chem. Phys.* **1995**, *196*, 47-58.
49. Perera, S. D.; Urquhart, S. G. Systematic Investigation of π-π Interactions in near-Edge X-Ray Fine Structure (NEXAFS) Spectroscopy of Paracyclophanes. *J. Phys. Chem. A* **2017**, *121*, 4907-4913.

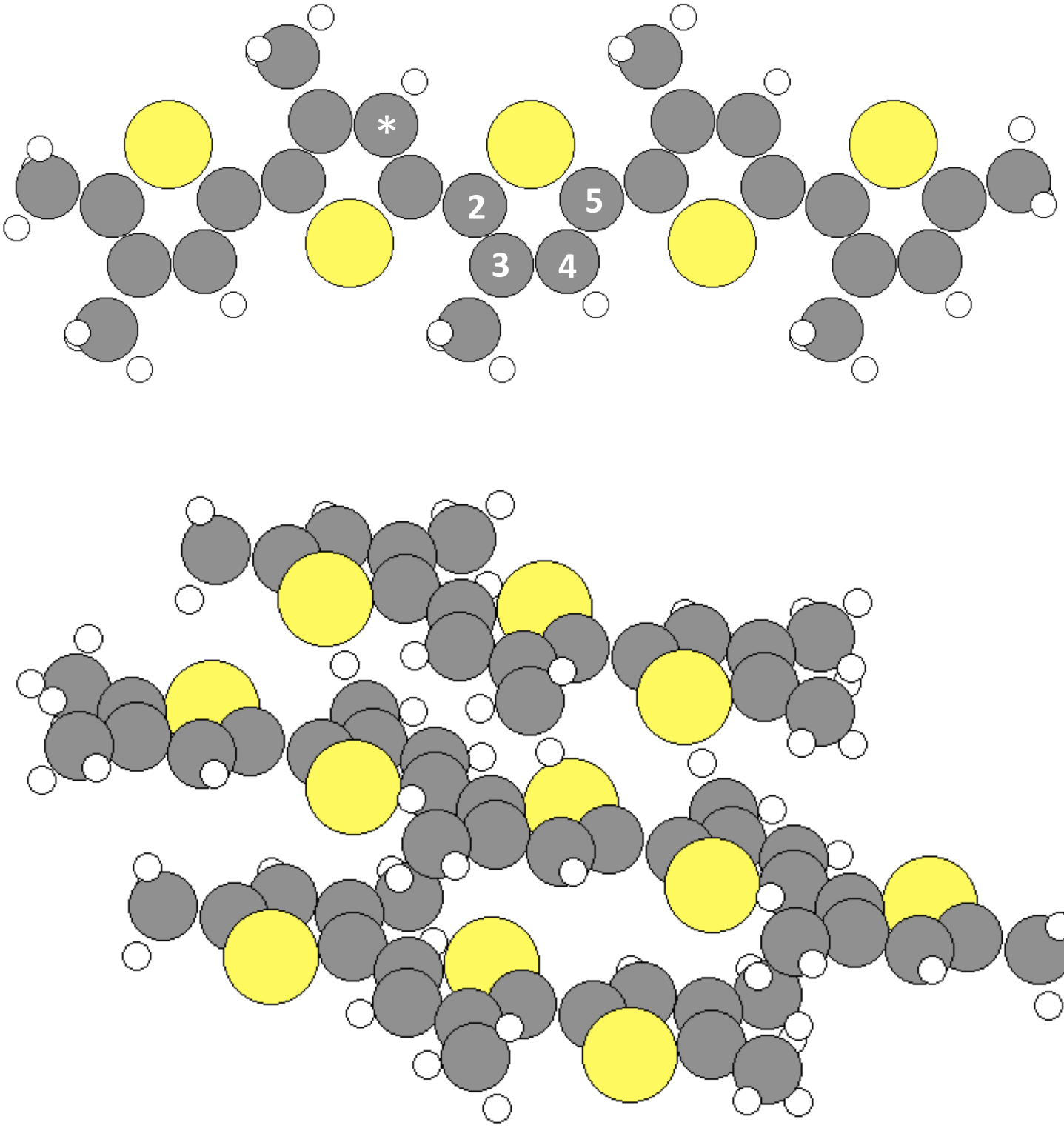

Scheme 1

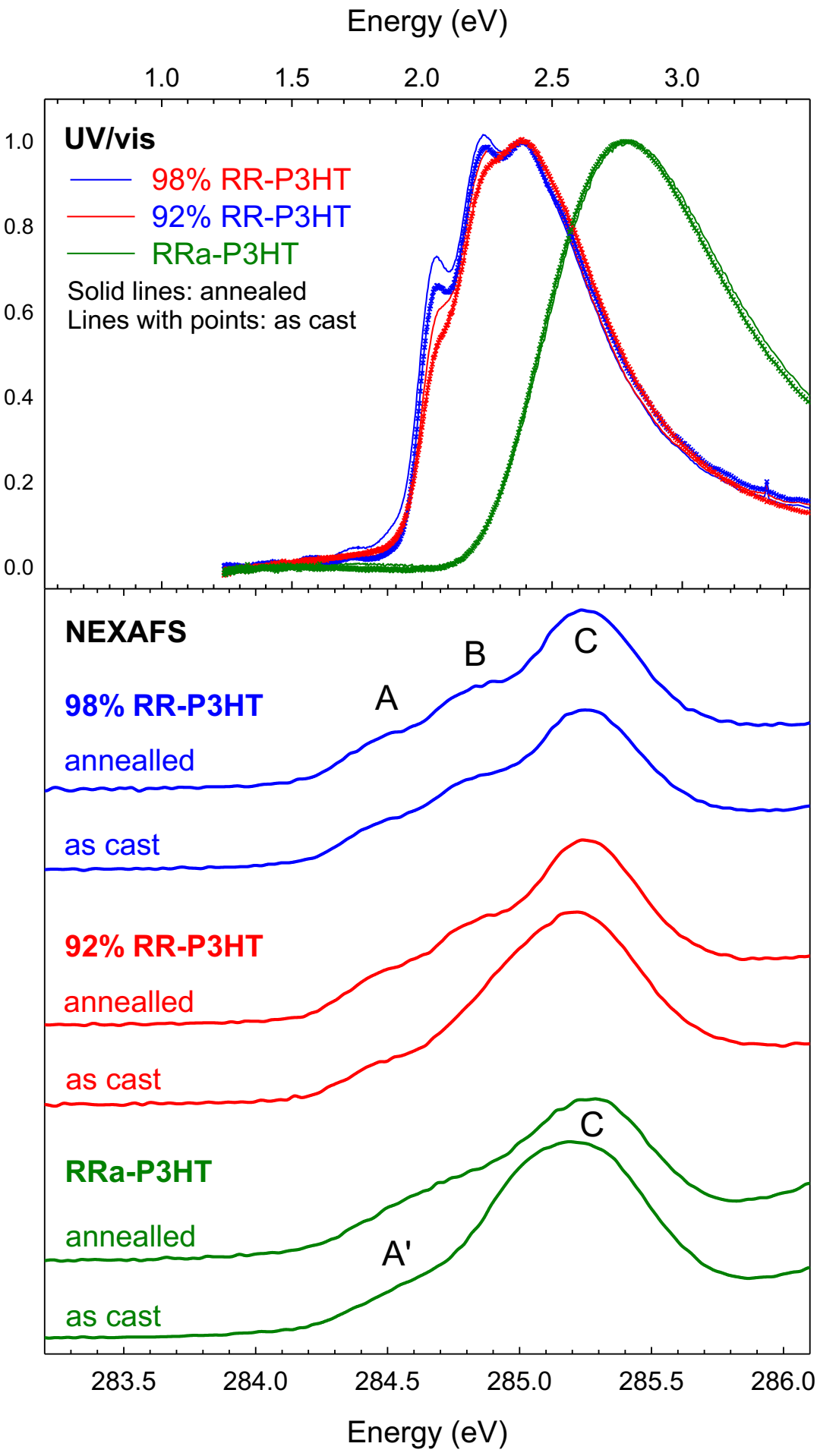
Energy (eV)
1.0
1.5
2.0
2.5
3.0
UV/vis
98% RR-P3HT
92% RR-P3HT
RRa-P3HT
Solid lines: annealed
Lines with points: as cast
1.0
0.8
0.6
0.4
0.2
0.0
NEXAFS
A
B
C
98% RR-P3HT
annealled
as cast
92% RR-P3HT
annealled
as cast
C
RRa-P3HT
annealled
A'
as cast
283.5
284.0
284.5
285.0
285.5
286.0
Energy (eV)

Figure 1

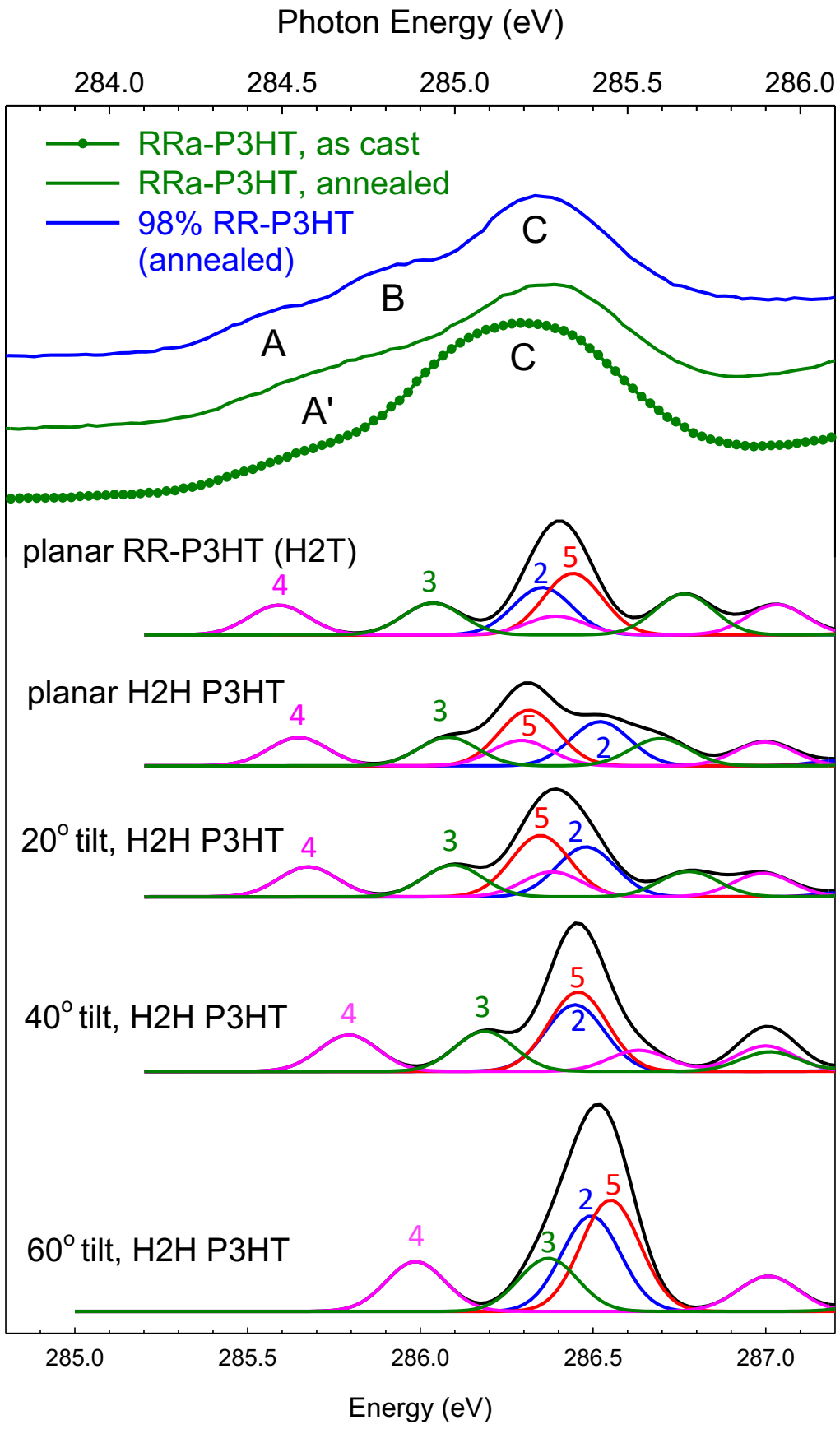
Photon Energy (eV)
284.0
284.5
285.0
285.5
286.0
RRa-P3HT, as cast
RRa-P3HT, annealed
98% RR-P3HT
(annealed)
A
A'
B
C
C
planar RR-P3HT (H2T)
planar H2H P3HT
20° tilt, H2H P3HT
40° tilt, H2H P3HT
60° tilt, H2H P3HT
2
3
4
5
285.0
285.5
286.0
286.5
287.0
Energy (eV)

Figure 2

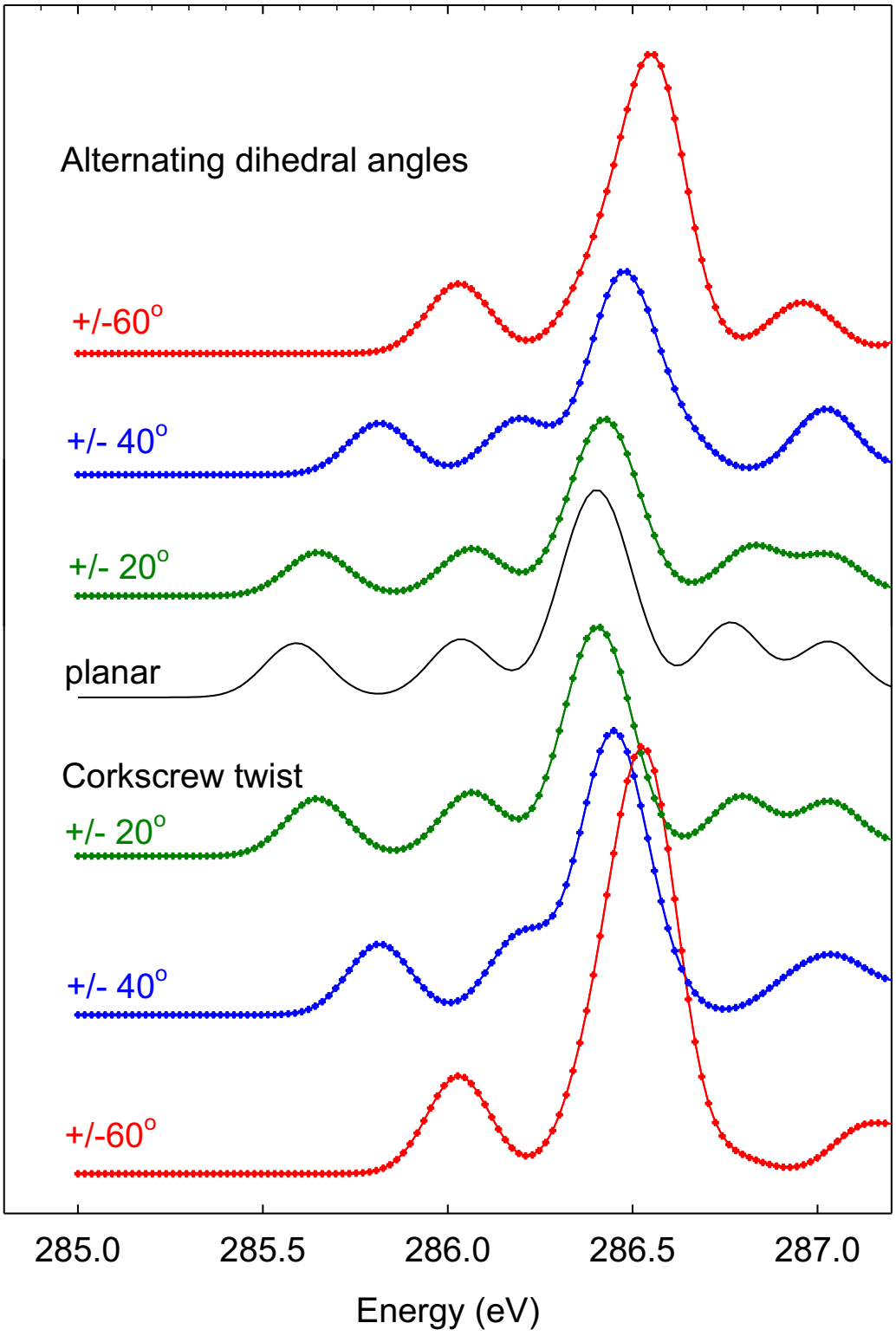
Alternating dihedral angles
+/-60°
+/- 40°
+/- 20°
planar
Corkscrew twist
+/- 20°
+/- 40°
+/-60°
285.0
285.5
286.0
286.5
287.0
Energy (eV)

Figure 3

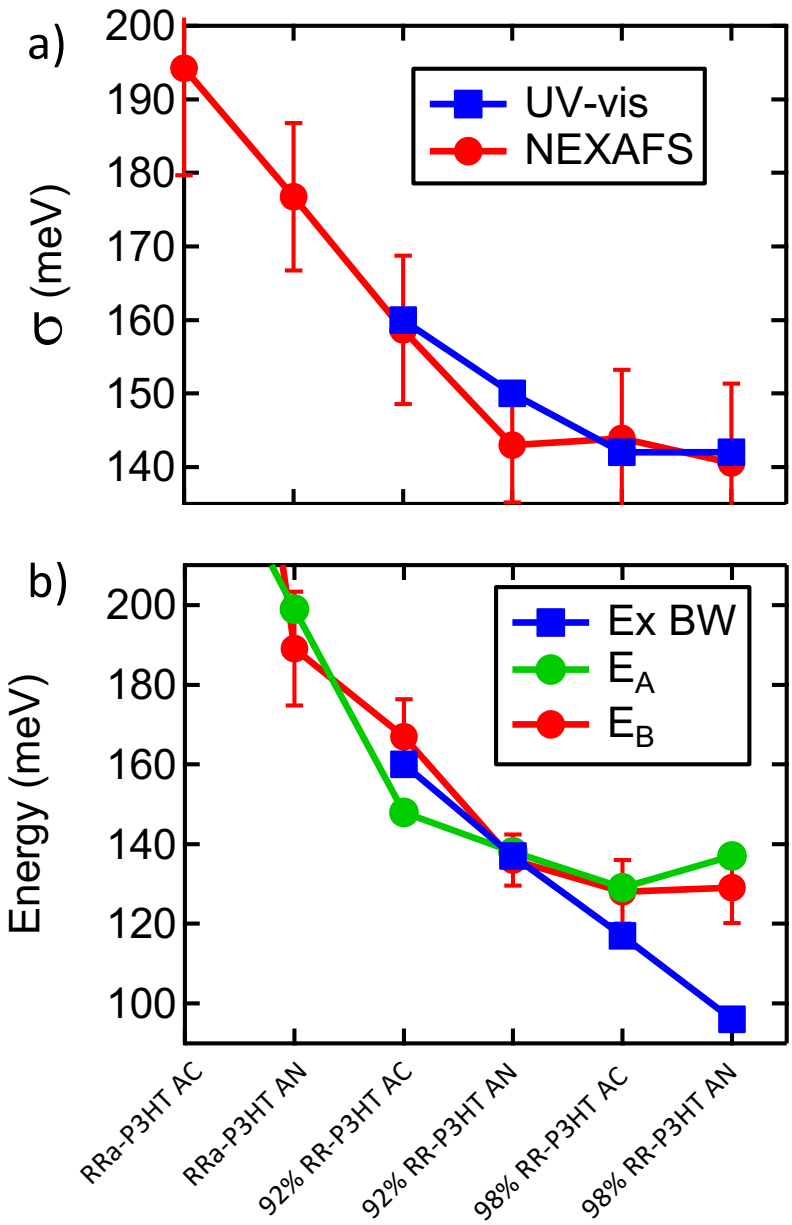
a)
σ (meV)
200
190
180
170
160
150
140
UV-vis
NEXAFS
b)
Energy (meV)
200
180
160
140
120
100
Ex BW
E_A
E_B
RRa-P3HT AC
RRa-P3HT AN
92% RR-P3HT AC
92% RR-P3HT AN
98% RR-P3HT AC
98% RR-P3HT AN

Figure 4

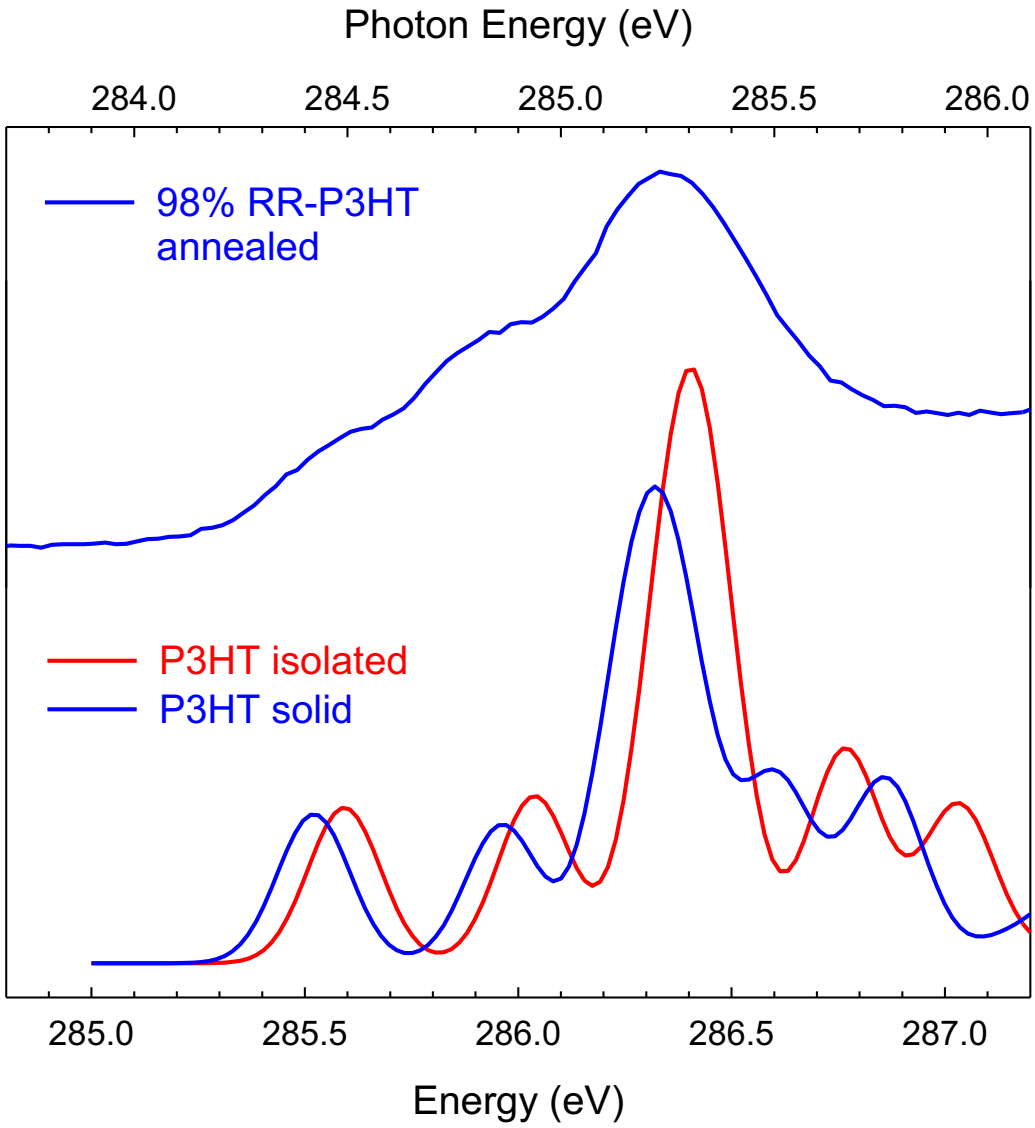
Photon Energy (eV)
284.0
284.5
285.0
285.5
286.0
98% RR-P3HT
annealed
P3HT isolated
P3HT solid
285.0
285.5
286.0
286.5
287.0
Energy (eV)

Figure 5

Supporting Information

Connecting Molecular Conformation to Aggregation in P3HT Using Near Edge X-ray Absorption Fine Structure Spectroscopy

Stephen G, Urquhart,[a,*] Mercedes Martinson,[a] Shaylin Eger,[a] Victor Murcia,[b] Harald Ade,[d] Brian A. Collins[b,c]

a. Department of Chemistry, University of Saskatchewan, Treaty Six Territory, Saskatoon, SK, Canada
b. Materials Science and Engineering Program, Washington State University, Pullman, WA
c. Department of Physics and Astronomy, Washington State University, Pullman, WA
d. Department of Physics, North Carolina State University, Raleigh, NC

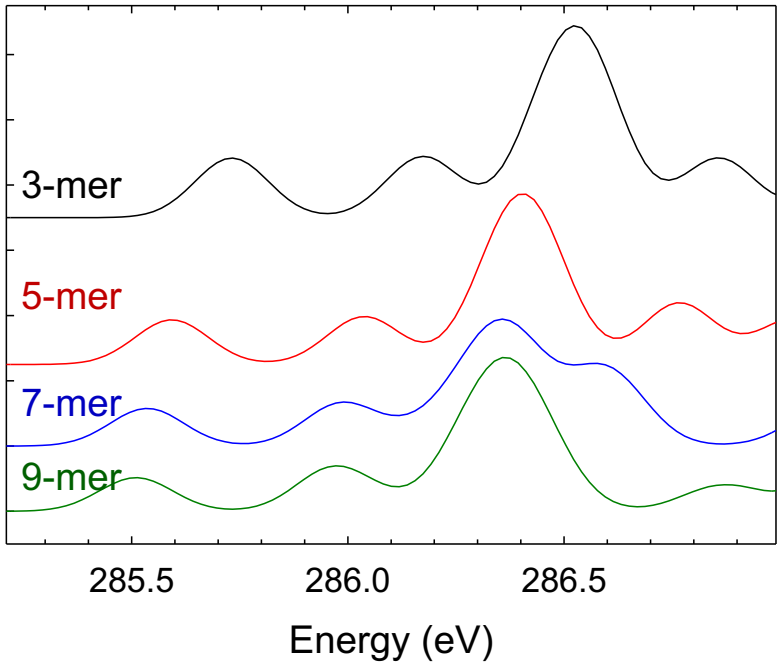

Figure S1: Carbon 1s NEXAFS spectra (π* band) of 3-methyl-thiophene trimer (3-mer), pentamer (5-mer), septamer (7-mer), and nonamer (9-mer).

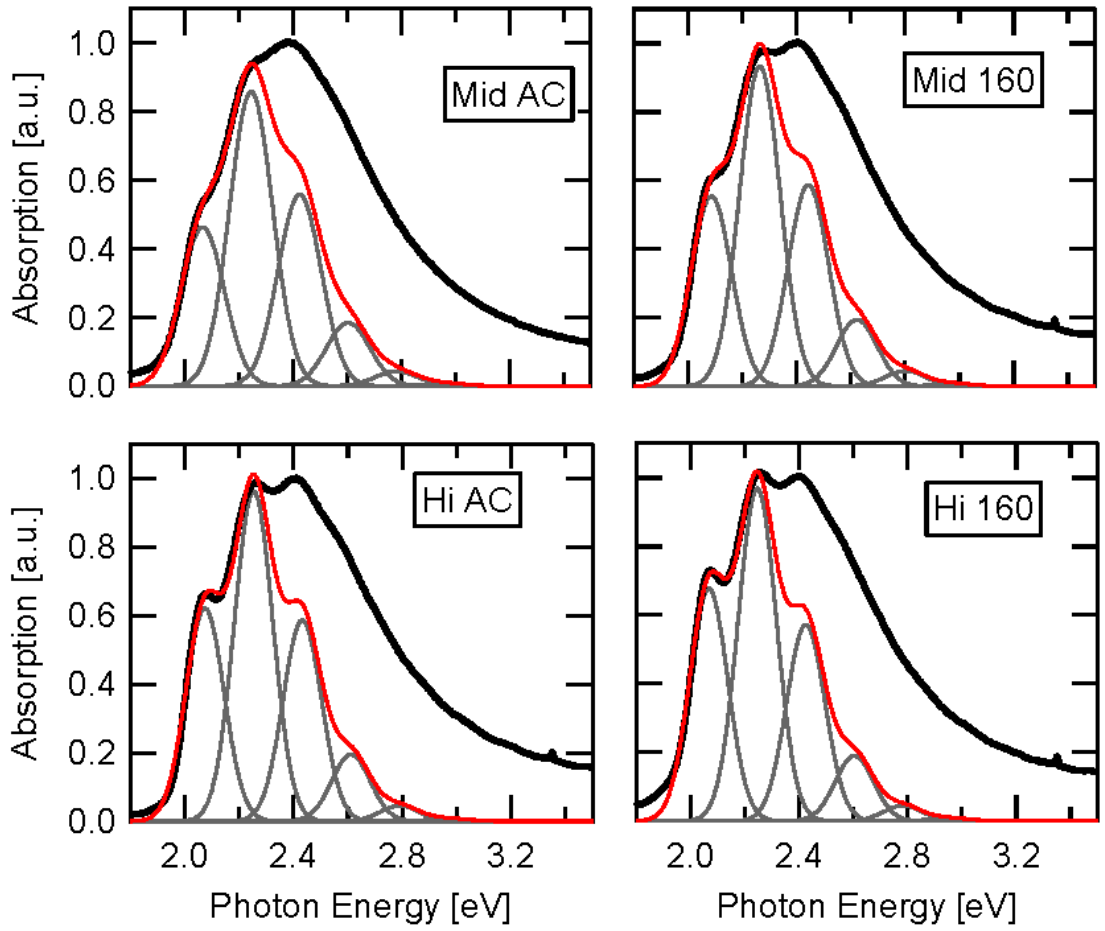

$$A(E) \propto \sum_{m=0}^{N} \left(\frac{e^{-S}S^{m}}{m!}\right)\left(1 - \frac{We^{-S}}{2E_p}\sum_{n\neq m}^{N}\frac{S^{n}}{n!\,(n-m)}\right)^{2} exp\left(\frac{\left(E - E_{0-0} - mE_p - \frac{1}{2}WS^{m}e^{-S}\right)^{2}}{2\sigma^{2}}\right)$$

Figure S2: Fits of UV/vis spectra to Spano model and the model used (Clark et al., Appl. Phys. Lett., 2009, 94, 163306)

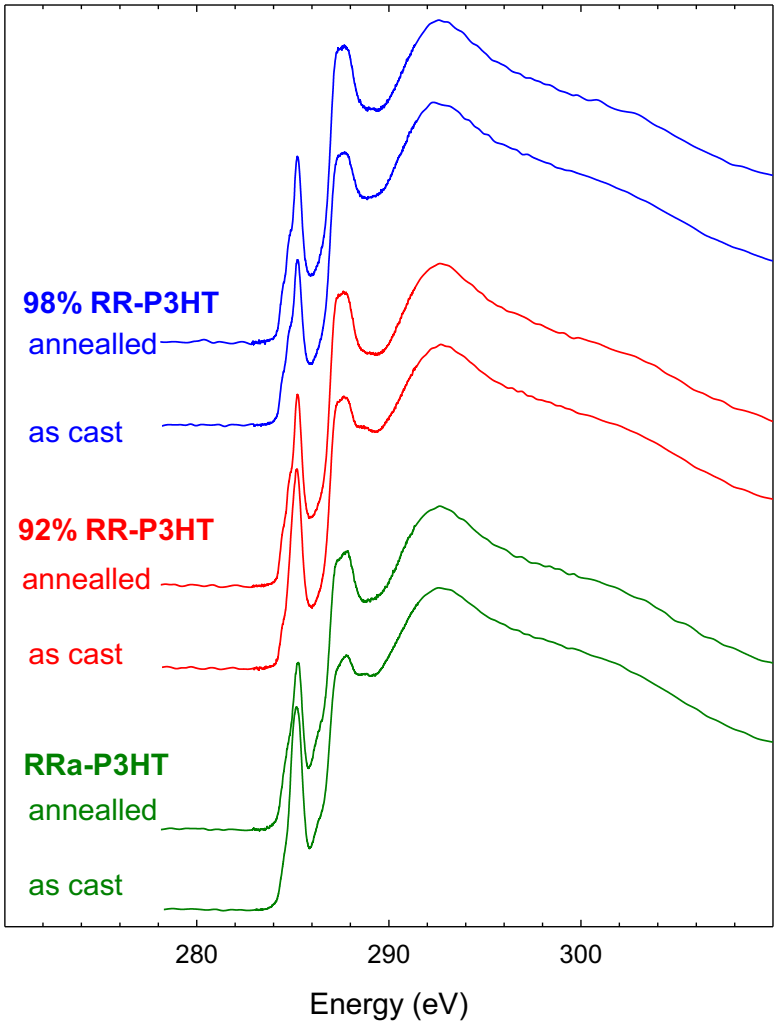

Figure S3: Carbon 1s NEXAFS spectra of regio-random poly(3-hexyl thiophene (RRa-P3HT; green traces) , 98% (blue traces) and 92% (red traces) regio-regular poly(3-hexyl thiophene) (RR-P3HT), in as cast and annealed form.

		98% RR-P3HT		92% RR-P3HT	
		As cast	Annealed	As cast	Annealed
A	Energy (eV)	284.47(2)	284.48(2)	284.49(2)	284.48
	Width (eV)	0.34(2)	0.33(3)	0.37(2)	0.34(2)
	Area	2,740±350	2,800±420	2,550±350	3,110±330
B	Energy (eV)	284.79	284.79	284.83	284.80
	Width (eV)	0.34(2)	0.33(2)	0.37(3)	0.34(2)
	area	4,610±440	4,930±520	3,560±730	5,250±430
C	Energy (eV)	285.25	285.24	285.22	285.25
	Width (eV)	0.52	0.52	0.59	0.51
	area	17,380±240	19,670±290	22,360±580	19,990±260

		RRa-P3HT	
		As cast	Annealed
A’	Energy (eV)	284.59(3)	284.54
	Width (eV)	0.46(3)	0.42
	Area	3,830±670	3,520±170
C[a]	Energy (eV)	285.04(2)	284.85
	Width (eV)	0.46(4)	0.42
	Area	13,920±2920	4,790±190
	Energy (eV)	285.37(3)	285.27
	Width (eV)	0.43(2)	0.52
	Area	11,090±2460	17,410±370

Table S1: Results of Fits of π* Band[a]

a. The width of peaks 0 and 1 are constrained to be equal, and the parameters of peak 3 are held to be identical in all 6 fits.

b. Peak C in RRa-P3HT is fit with two Gaussian peaks

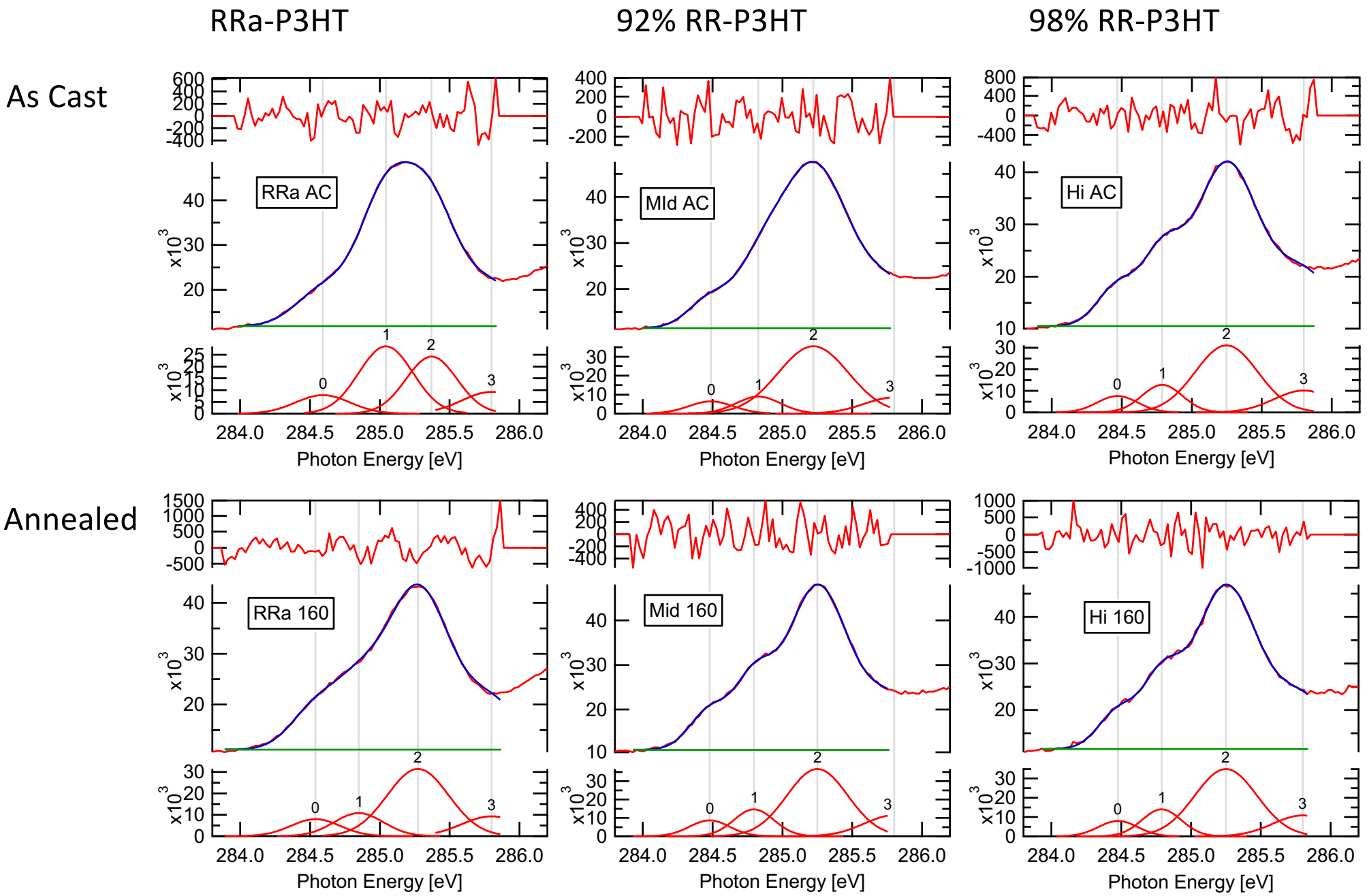

Figure S4: Fits of the Carbon 1s → π*-band for RRa-P3HT (left) , 92%-RR-P3HT (center) and 98%-RR-P3HT (right), in as cast (top row) and annealed form (bottom row)

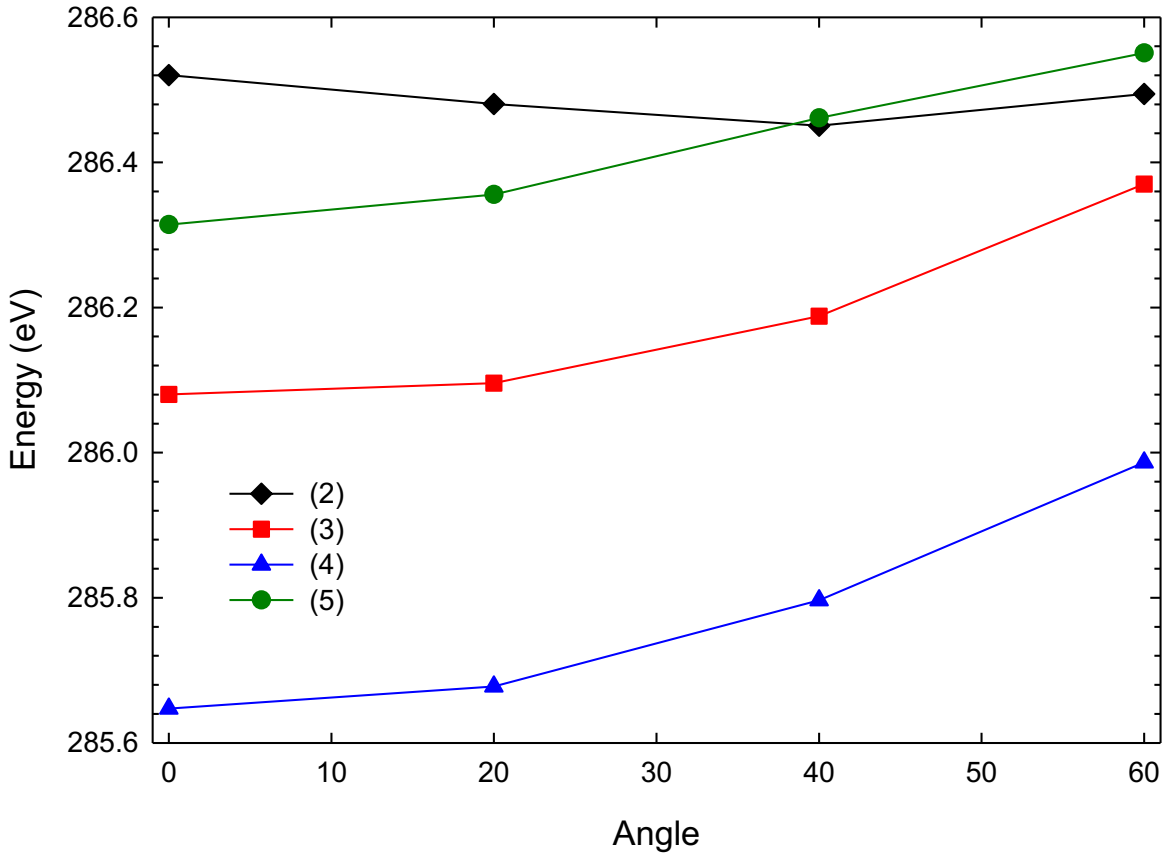

Figure S5: Energy of the four lowest energy carbon 1s → π* transitions in the H2T P3HT model (derived from Figure 3) as a function of modification of the S-C-C-S dihedral angle. Transitions are identified by the IUPAC site numbers (2, 3, 4 and 5).

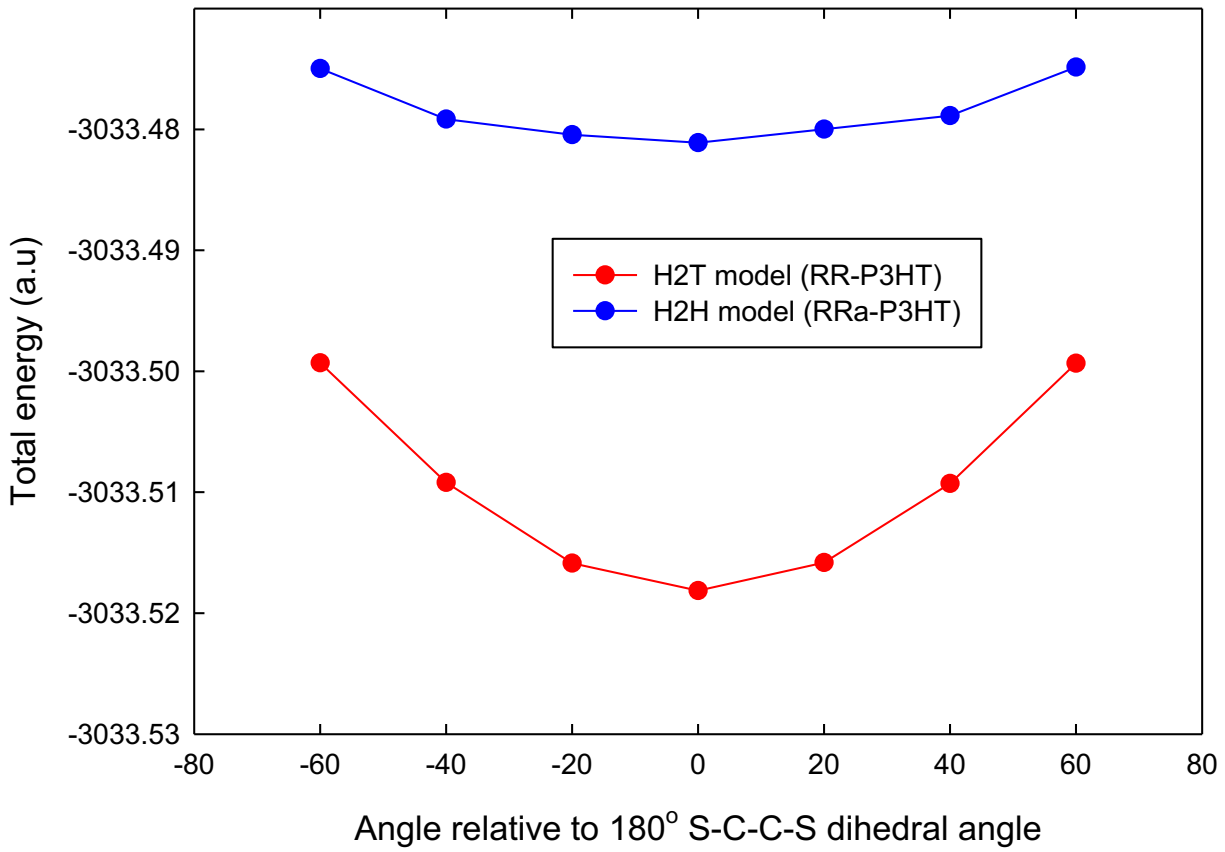

Figure S6: Calculations of the total energy of the head-to head and the head-to-tail P3HT models as a function of modification of the S-C-C-S dihedral angle. Models were the same as that used for Figure 2; calculations were performed in the ground state, with the same DFT functional and basis sets.